

$$\begin{aligned} \chi_n(z) &= A \cos kz, & \text{for } |z| < L/2 \\ &= B \exp[-\kappa(z - L/2)], & \text{for } z > L/2 \\ &= B \exp[+\kappa(z + L/2)], & \text{for } z < -L/2 \end{aligned} \quad (2)$$

or

$$\begin{aligned} \chi_n(z) &= A \sin kz, & \text{for } |z| < L/2, \\ &= B \exp[-\kappa(z - L/2)], & \text{for } z > L/2 \\ &= B \exp[+\kappa(z + L/2)], & \text{for } z < -L/2 \end{aligned} \quad (3)$$

where

$$\epsilon_n = \frac{\hbar^2 k^2}{2m_A^*} - V_0, \quad \epsilon_n = -\frac{\hbar^2 \kappa^2}{2m_B^*}, \quad -V_0 < \epsilon < 0 \quad (4)$$

For the solution of Eq. (2), the continuity conditions at  $z = \pm L/2$  yield

$$A \cos(kL/2) = B$$

$$(k_A/m_A^*) \sin(kL/2) = \kappa B/m_B^*$$

$$S = \frac{\hbar}{2m} (\bar{\psi} \nabla \psi - \nabla \bar{\psi} \psi)$$

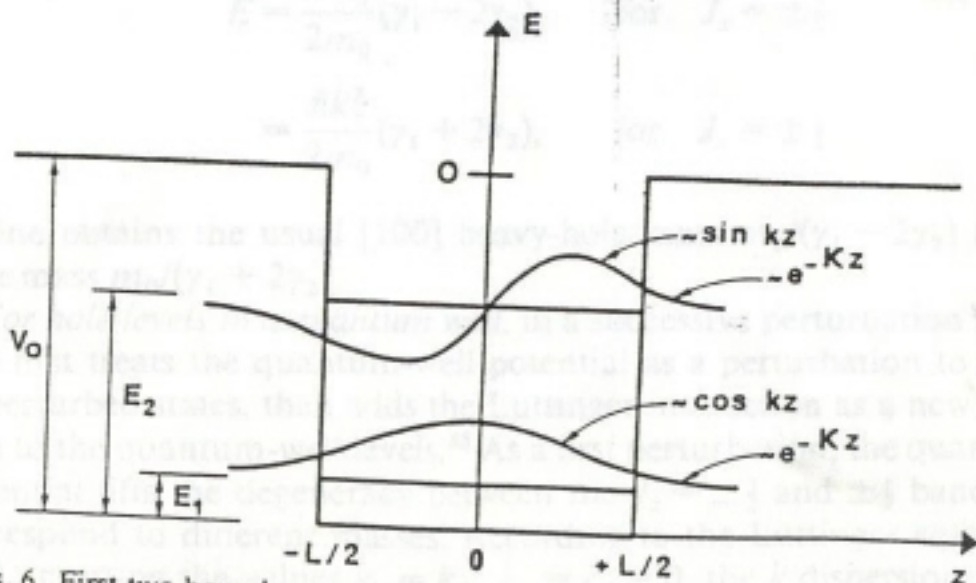


FIG. 6. First two bound energy levels and wave functions in a finite quantum well.

Therefore

$$(k/m_A^*) \tan(kL/2) = \kappa/m_B^* \quad (5)$$

Similarly, Eq. (3) yields

$$k/m_A^* \cotan(kL/2) = -\kappa/m_B^* \quad (6)$$

The equations can be solved numerically or graphically. A very simple graphical type of solution can be developed if  $m_A^* = m_B^*$ . Then, using Eq. (4), Eqs. (5) and (6) can be transformed into implicit equations in  $k$  alone:

$$\cos(kL/2) = k/k_0, \quad \text{for } \tan kL/2 > 0 \quad (7)$$

$$\sin(kL/2) = k/k_0, \quad \text{for } \tan kL/2 < 0 \quad (8)$$

where

$$k_0 = 2m^*V_0/\hbar^2 \quad (9)$$

These equations can be visualized graphically (Fig. 7). There is always one bound state. The number of bound states is

$$1 + \text{Int} \left[ \left( \frac{2m_A^*V_0L^2}{\pi^2\hbar^2} \right)^{1/2} \right] \quad (10)$$

where  $\text{Int}[x]$  indicates the integer part of  $x$ .

The important limiting case of the *infinitely high barriers* (Fig. 5) can be found again by putting  $k_0 = \infty$  in Fig. 7. There is then an infinity of bound states with  $k = n\pi/L$ . Even solutions are  $\chi_n \sim \cos kz$ , with  $kL = (2n+1)\pi$ ; odd solutions are  $\chi_n \sim \sin kz$ , with  $kL = 2n\pi$ .  $\chi_n$  even and  $\chi_n$  odd are the

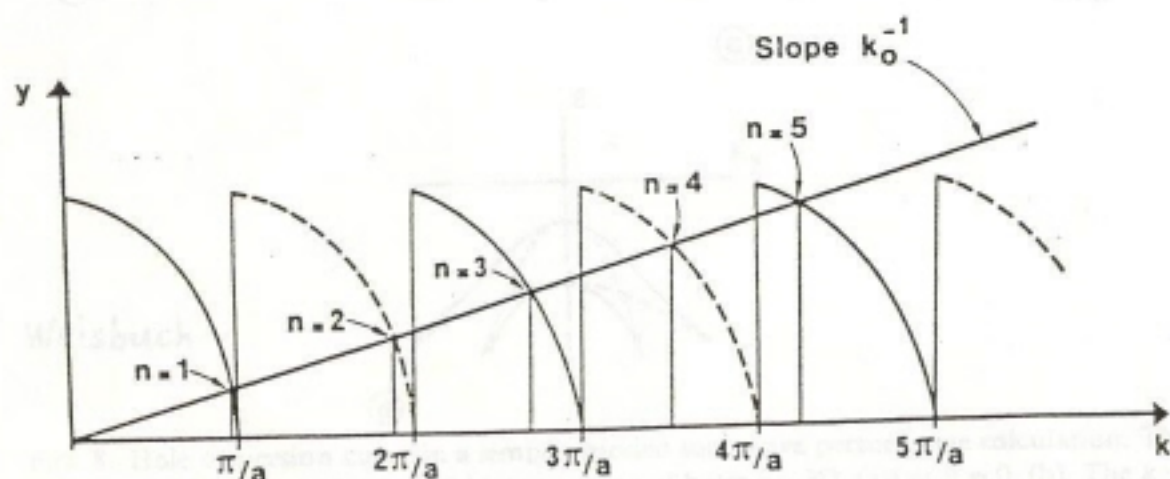


FIG. 7. Graphical solution for Eqs. (7) and (8). Solutions are located at the intersections of the straight line with slope  $k_0^{-1}$  with curves  $y = \cos kL/2$  (with  $\tan kL/2 > 0$ ; —; even wave functions) or  $y = \sin kL/2$  (with  $\tan kL/2 < 0$ ; - - -; odd solutions).

## b. Hole Energy Levels

Turning to the hole quantization problem, the situation is much more complicated in usual semiconductor materials. The bulk hole bands are described in the Kane model by basis functions with angular momentum  $J = \frac{3}{2}$  symmetry, i.e., 4-fold degeneracy at  $k = 0$  (neglecting the spin-orbit split-off valence band).

The dispersion near  $k = 0$  can be described by the Luttinger Hamiltonian<sup>84a</sup>:

$$H = \frac{\hbar^2}{2m_0} [(\gamma_1 + \frac{1}{2}\gamma_2)k^2 - 2\gamma_2(k_x^2J_x^2 + k_y^2J_y^2 + k_z^2J_z^2) - 4\gamma_3((k_x \cdot k_y)\{J_x \cdot J_y\} + \dots)] \quad (11)$$

where  $\gamma_1, \gamma_2, \gamma_3$  are the Luttinger parameters of the valence band and the symbol  $\{ \cdot \}$  represents the anticommutation

$$\{k_x \cdot k_y\} = k_x k_y + k_y k_x$$

In the bulk, propagation in a given direction can be described in terms of heavy- and light-hole propagation. Taking as a quantization axis  $z$  for the angular momentum the direction of propagation of the hole, the levels  $J_z = \pm \frac{3}{2}$  and  $J = \pm \frac{1}{2}$  give a simple dispersion relation from Eq. (11). Taking for example  $k_z$  in a [100] direction, the kinetic energy of holes is

$$E = \frac{\hbar^2 k_z^2}{2m_0} (\gamma_1 - 2\gamma_2), \quad \text{for } J_z = \pm \frac{3}{2}$$

$$= \frac{\hbar^2 k_z^2}{2m_0} (\gamma_1 + 2\gamma_2), \quad \text{for } J_z = \pm \frac{1}{2} \quad (12)$$

One obtains the usual [100] heavy-hole mass  $m_0/(\gamma_1 - 2\gamma_2)$  and light-hole mass  $m_0/(\gamma_1 + 2\gamma_2)$ .



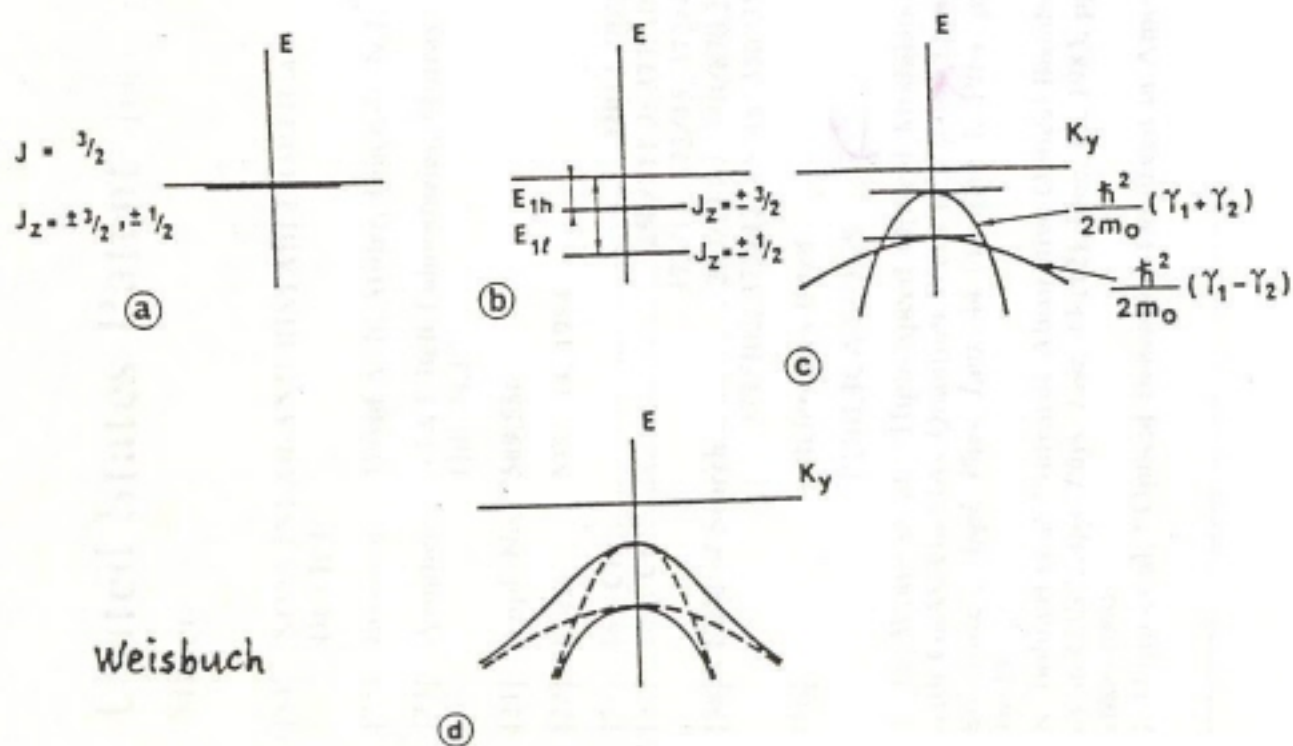
direction *perpendicular* to  $z$  is then given by

$$E = \frac{\hbar^2 k_{\perp}^2}{2m_0} (\gamma_1 + \gamma_2), \quad \text{for } J_z = \pm \frac{3}{2} \quad (12a)$$

$$E = \frac{\hbar^2 k_{\perp}^2}{2m_0} (\gamma_1 - \gamma_2), \quad \text{for } J_z = \pm \frac{1}{2}$$

The transverse dispersion equation corresponding to  $J_z = \pm \frac{3}{2}$  (*heavy-hole band along the  $z$  direction*), now has a *light mass* ( $m_0/\gamma_1 + \gamma_2$ ), whereas the  $J_z = \pm \frac{1}{2}$  level now has a *heavy mass* (Fig. 8). This situation is quite similar to that developed under a uniaxial compressive stress in the [100] direction.<sup>86</sup> The difference here is that the  $\frac{3}{2}$  band is the higher-lying one. Due to the lighter mass of the  $\frac{3}{2}$  band, one initially expects a crossing of the two bands. However, higher-order  $\mathbf{k} \cdot \mathbf{p}$  perturbation terms lead to an anticrossing behavior, which increases the "heavy-hole" band mass and decreases the "light-hole" band mass.

Actually, the above procedure, which describes qualitatively the complicated valence-band effects, is not correct. One has to treat on equal footing the  $\mathbf{k} \cdot \mathbf{p}$  perturbation, which yields the dispersion, and the dimensional perturbation (d.w.).



의 기능을 빛으로 구현할 수 있는 바, 미래의 광컴퓨터 등의 광정보기기의 핵심소자가 된다.

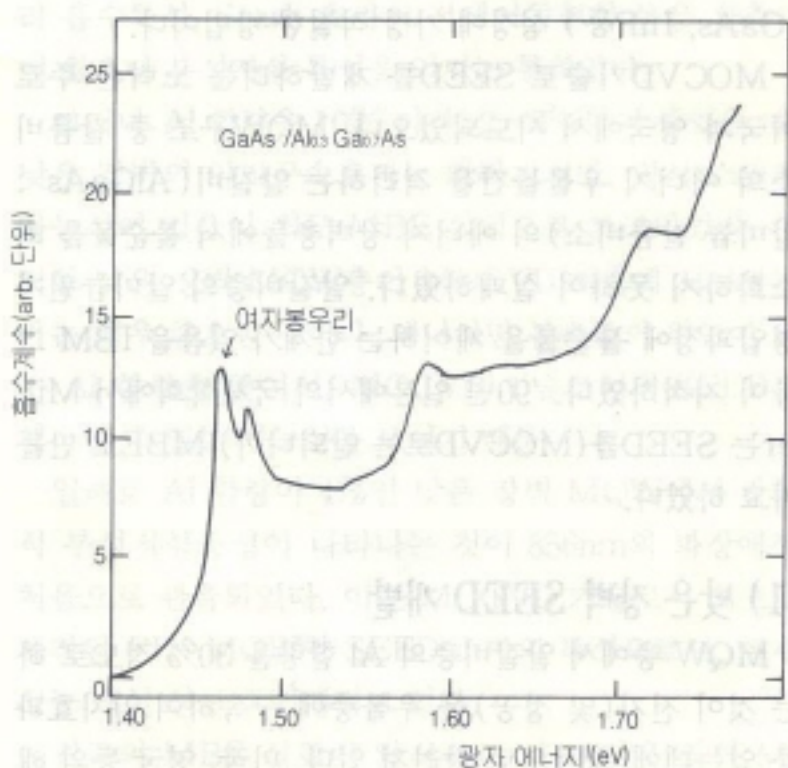
SEED는 '84년에 Bell연구소가 처음 개발하였지만 그 뿌리는 오래전에 심었었다. '50년대의 레이저 기초 연구, '60년대의 각종 레이저 개발과 함께 '62년의 갈륨비소 반도체 레이저 연구와 '60년대 중반이후의 광섬유 개발 등은 '70년대 광통신기술을 성숙케 하였다.

이 밑거름으로 '70년경, 광집적회로의 원시적 개념과 안정점이 2개인 광쌍안정성(Optical Bistability)이라는 광스위치 개념이 배태되는데, 같은 시기에 IBM의 Esaki는 초격자(Super-lattice)내지는 다중양자우물(Multiple Quantum Well : MQW)이라는 인공반도체구조의 개념과 터널소자의 응용을 제안하였다.

한편, MQW 구조에 관한 광특성연구가 '70년대 중반 Bell에서 주도되고, MQW 구조의 반도체 성장으로는 분자선결정성장법(MBE)을 사용하였었다. 일례로 갈륨비소(GaAs : 갈비)와 알루미늄갈륨비소(AlGaAs : 알갈비)의 반도체층들을 갈비 / 알갈비 / 갈비 / 알갈비 / 갈비...로 수십층 성장하여 MQW를 만드는데, 한층이 100Å 정도이니 머리카락의 일만분의 일 두께가 된다.

Bell에서는 갈비 / 알갈비 MQW 구조에서 주로 전자와 정공(Hole)이 결합하여 순간적으로 생성되는 여자(Exciton)라는 양자의 광특성을 저온에서 측정할 수

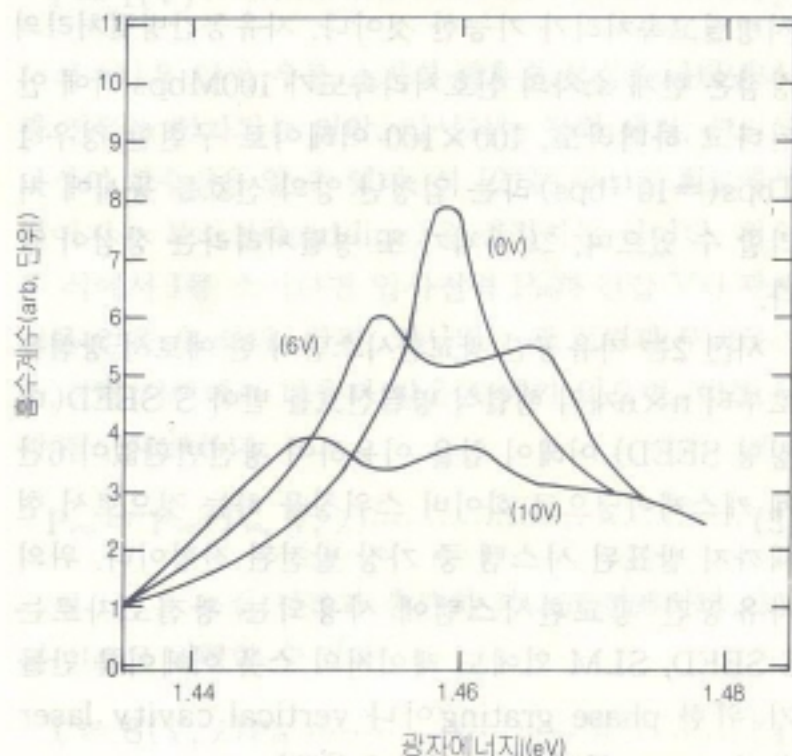
〈그림 1〉 광 흡수 스펙트럼



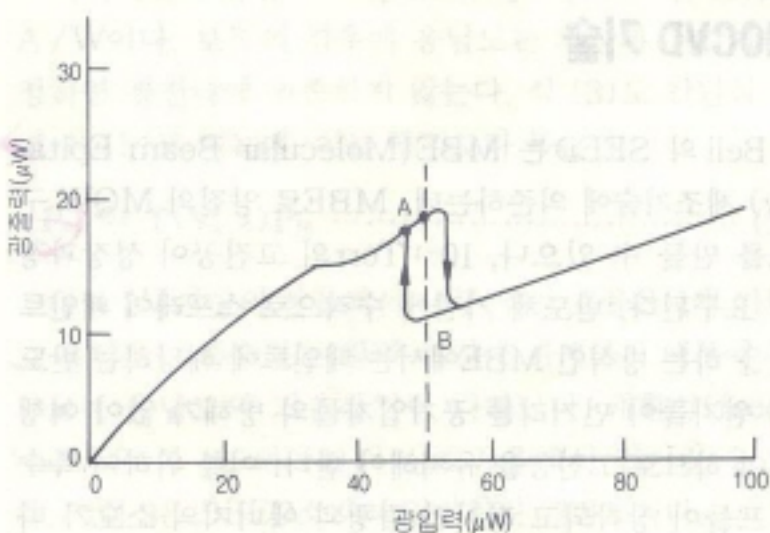
있었는데, 이것이 MBE 기술의 발전으로서 '80년대초에는 상온에서 여자들을 관측하게 되었다. 그런 MQW 구조를 PIN 소자의 중간인 I층에 구현하여 실용적인 광스위치 소자를 개발한 공로는 Bell의 젊은 물리학자 David Miller에게로 귀착하였다. 그는 이 소자를 SEED로 명명하였다(그림 1 참조).

PIN 구조에 전계를 가하면 여자의 광흡수봉우리가 이동하여 골짜기가 되는 Stark 양자효과가 발생하고, 적당한 부하가 있는 회로를 구성하여 레환성을 유도하며, 광학적인 부성저항 특성을 갖는 SEED는 마침내 광스위치가 되는 것이다(그림 2 (a), (b) 참조).

광스위치가 되기 위한 광쌍안정성은 '70년대 기체·액체·고체 레이저의 광쌍안정성 연구로부터 유래한다. 이 광쌍안정성 연구는 광학적으로 유도되는 광쌍안정성(그림 2)



(a) 양자 구속 스타크 효과(QCSE)



(b) 광입력-출력(광쌍안정표시 A, B)



액체·고체 형태의 여러가지 광학적 비선형 물질들을 탐색하며 연구되었으나 SEED야말로 상온에서 반도체 소자로서 동작하는 소자이므로 기존의 반도체 제조기술로 집적화가 가능하여 각광을 받게 되는 것이다.

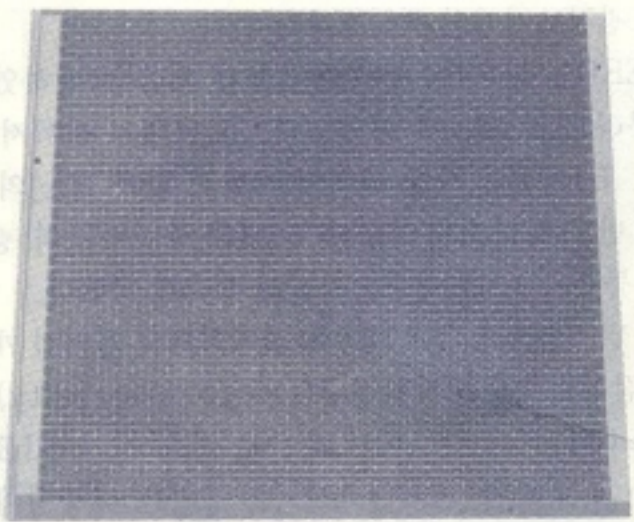
그후 Bell Lab.은  $n \times n$ 형 SEED-array 개발연구를 계속하여 '90년에는  $64 \times 32$  SEED chip을 개발하고, 시판에 착수하기에 이르렀다. 이는 광정보처리 소자 및 시스템의 고속성, 소형화, 집적화, 자유공간통신화,  $n \times n$ 형 직접병렬처리에 활로를 개척한 것이며, OEIC기술의 광정보산업화를 촉진하는 계기가 된다(사진 1 참조).

특히, 전자의 유선신호전달로서는 엄두를 낼 수 없는 대량의 자유공간 광접속이  $n \times n$ 형으로 수행 가능함으로서, '90년대 중반이후 등장할 광대역 ISDN, Intelligent layer 수준의 광교환 및 광컴퓨터에 필수적인 동시병렬고속처리가 가능한 것이다. 자유공간병렬처리의 장점은 한개 소자의 신호처리속도가 100Mbps 밖에 안 된다고 하더라도,  $100 \times 100$  어레이로 구현할 경우 1 Tbps(=10<sup>12</sup>bps)라는 엄청난 양의 신호를 동시에 처리할 수 있으며, 그 자체가 또 병렬처리라는 장점이 있다.

사진 2는 자유공간 광교환시스템의 한 예로서 광섬유로부터  $n \times n$ 개의 행렬식 병렬신호를 받아 S-SEED(대칭형 SEED) 어레이 칩을 이용하여 광전변환없이 6단계 캐스케이딩으로 화이버 스위칭을 하는 것으로서 현재까지 발표된 시스템 중 가장 발전된 전형이다. 위의 자유공간 광교환시스템에 사용되는 광전소자로는 S-SEED, SLM 외에도 레이저의 스폿 어레이를 만들기 위한 phase grating이나 vertical cavity laser diode array 등이 있다(사진 3 참조).

## MOCVD 기술

Bell의 SEED는 MBE(Molecular Beam Epitaxy) 제조기술에 의존하는데, MBE로 양질의 MQW 구조를 만들 수 있으나, 10<sup>-11</sup>Torr의 고진공이 성장과정에 요구된다. 반도체 기판에 수직으로 스프레이 페인트 칠을 하는 방식인 MBE에서는 페인트에 해당하는 반도체 원자들이 먼거리를 공기입자들의 방해가 없이 여행해야 하므로 고진공을 유지해야 한다. 이를 위하여 특수 펌프들이 장착되고 장시간 펌핑과 에너지의 소모가 따른다.



64 x 32 S-SEED Array (1.3 mm)<sup>2</sup>

그래서 유기금속기상결정성장법(MOVPE=Metalorganic Vapor Phase Epitaxy=MOCVD=Metal-organic Chemical Vapor Deposition)이라는 반도체 성장기술을 사용하여 소자들을 제작하려는 욕구가 따르기 마련인데, MOCVD는 반응기체 주입전에 저진공만 유지하면 되므로 기계펌프(와확산펌프)만으로 충분하며, 시간과 에너지를 절약할 수 있다. 게다가 MOCVD는 문자 그대로 유기금속화합물과 수소화합물 등의 열화학적 분해반응을 통하여 반도체를 성장하므로, 반도체 기판전체는 물론 여러 개의 기판에 동시성장하는 대량생산이 가능하고, 다양한 화합물 반도체(GaAs, InP등) 성장에 가장 적절한 방법이다.

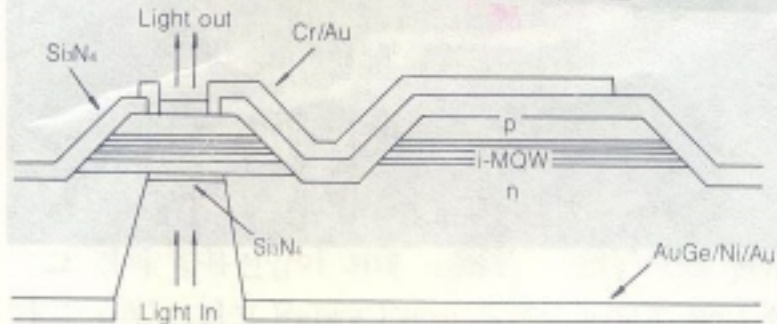
MOCVD기술로 SEED를 개발하려는 노력은 주로 미국과 영국에서 시도되었으나, MQW구조 중 갈륨비소의 에너지 우물들간을 격리하는 알갈비(AlGaAs : 알루미늄 갈륨비소)의 에너지 장벽층들에서 불순물을 최소화하지 못하여 실패하였다. 알갈비층의 알루미늄원자 영입과정에 불순물을 제어하는 한계가 있음을 IBM 그룹이 지적하였다. '90년 일본에서의 국제학회에서 Miller는 SEED를(MOCVD로는 안되니까) MBE로 만들자고 하였다.

### (1) 낮은 장벽 SEED 개발

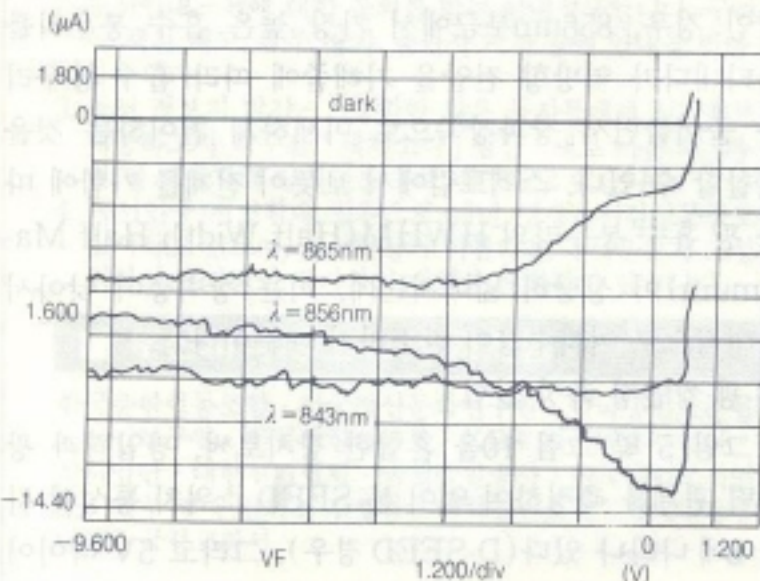
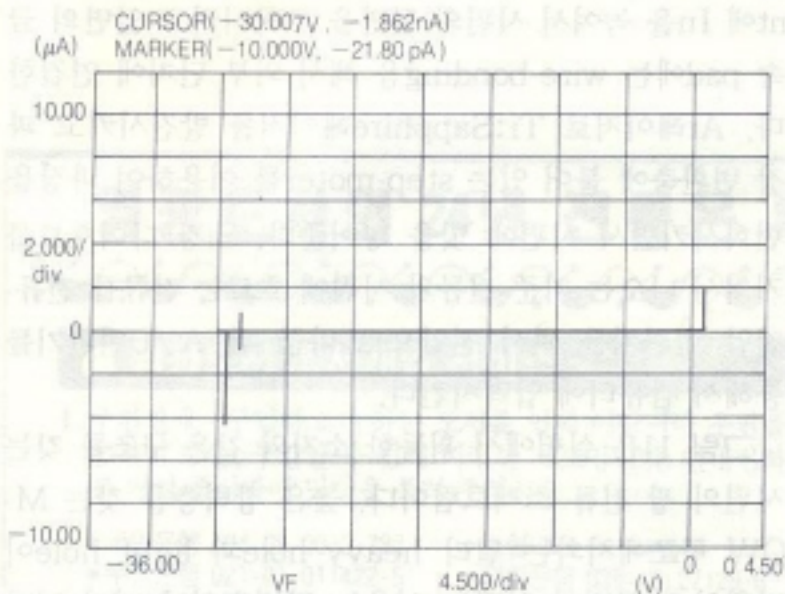
MQW 층에서 알갈비층의 Al 함량을 30% 정도로 하는 것이 전자(및 정공)을 우물층에 구속하여 양자효과를 얻는데에 최적으로 알려져 있다. 미국, 영국 등의 해



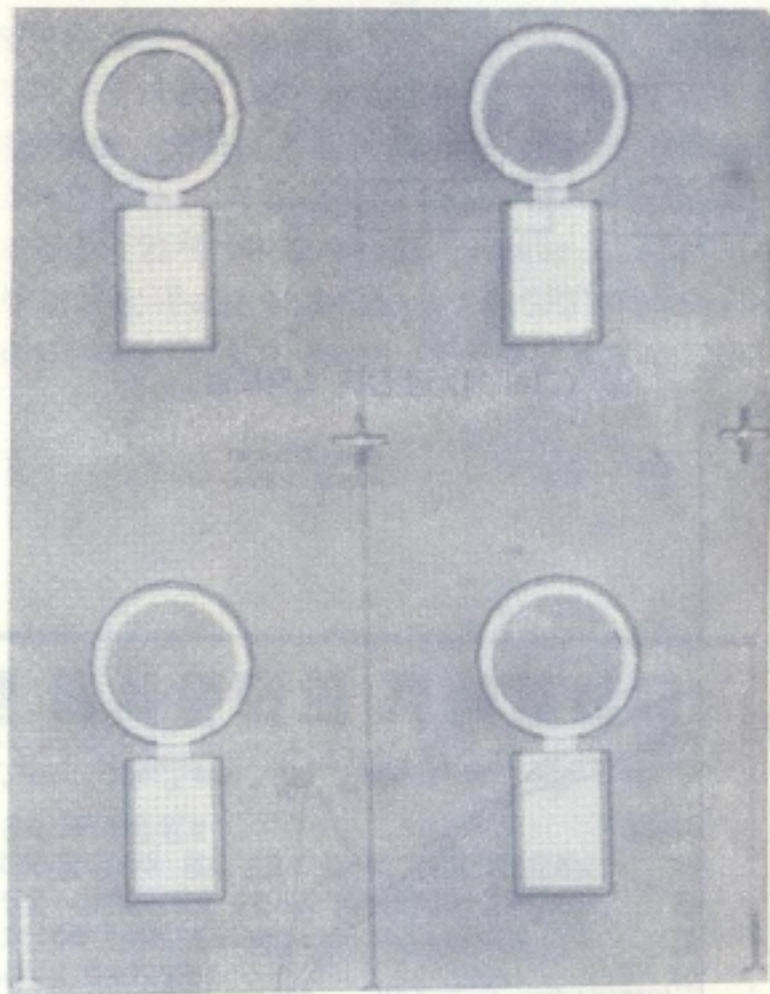
〈그림 8〉 투과형 SEED 소자의 단면도



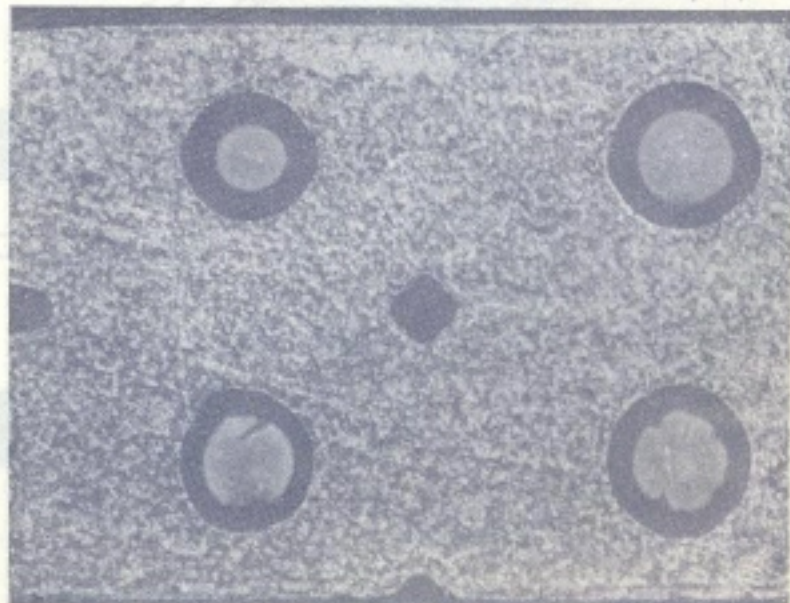
〈그림 9〉



〈사진 4〉 P금속 증착후의 앞면 모습(직경300μm)



〈사진 5〉 습식 식각 직후의 뒷면 사진(직경 200μm)





APL 62 (1993)  
 SPIE U.1813, 91 (1992)

The I-V characteristics illustrated in Fig.4 indicate the diode's responsivity, or the optical negative resistance obtained with an incident beam of 856nm wavelength. The exciton peak actually observed from the current LBQW pin structure was located at 857.2nm as shown in the photocurrent spectra, Fig.5.

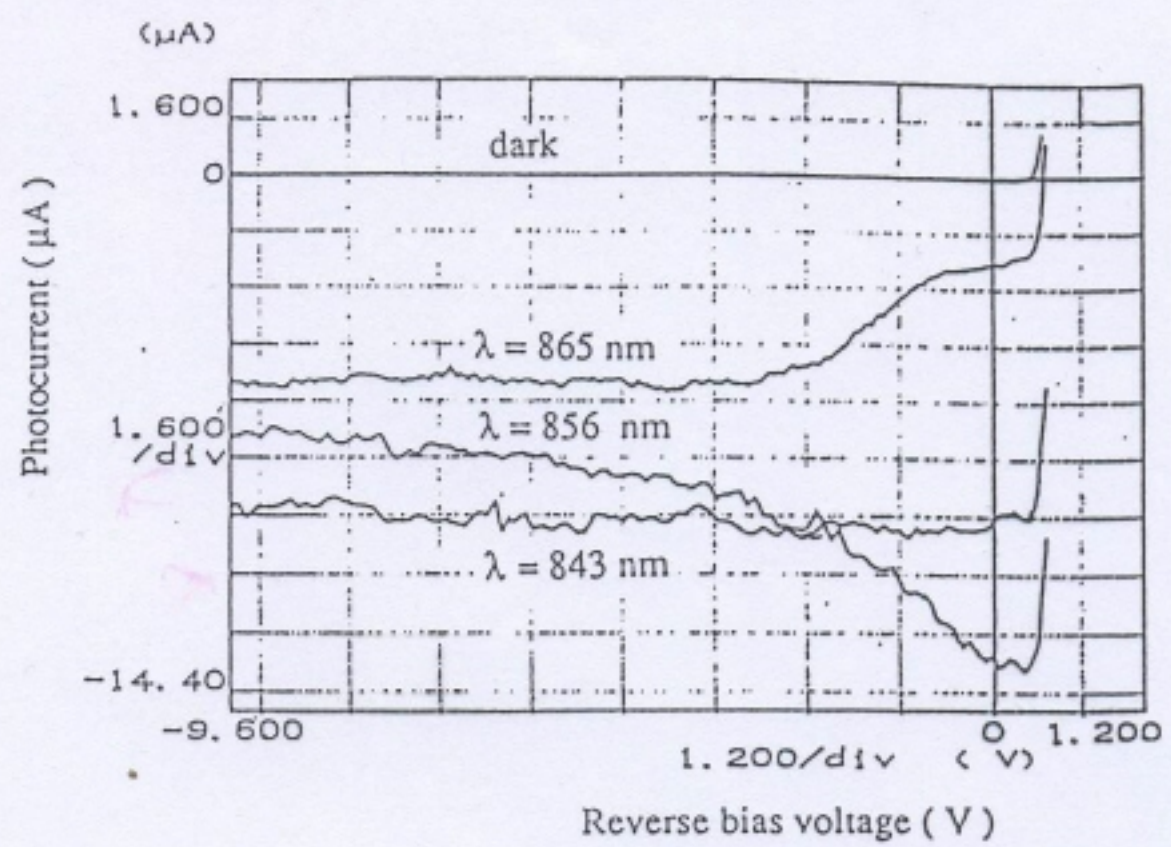


Fig. 4 Optical I-V curves at different wavelengths.

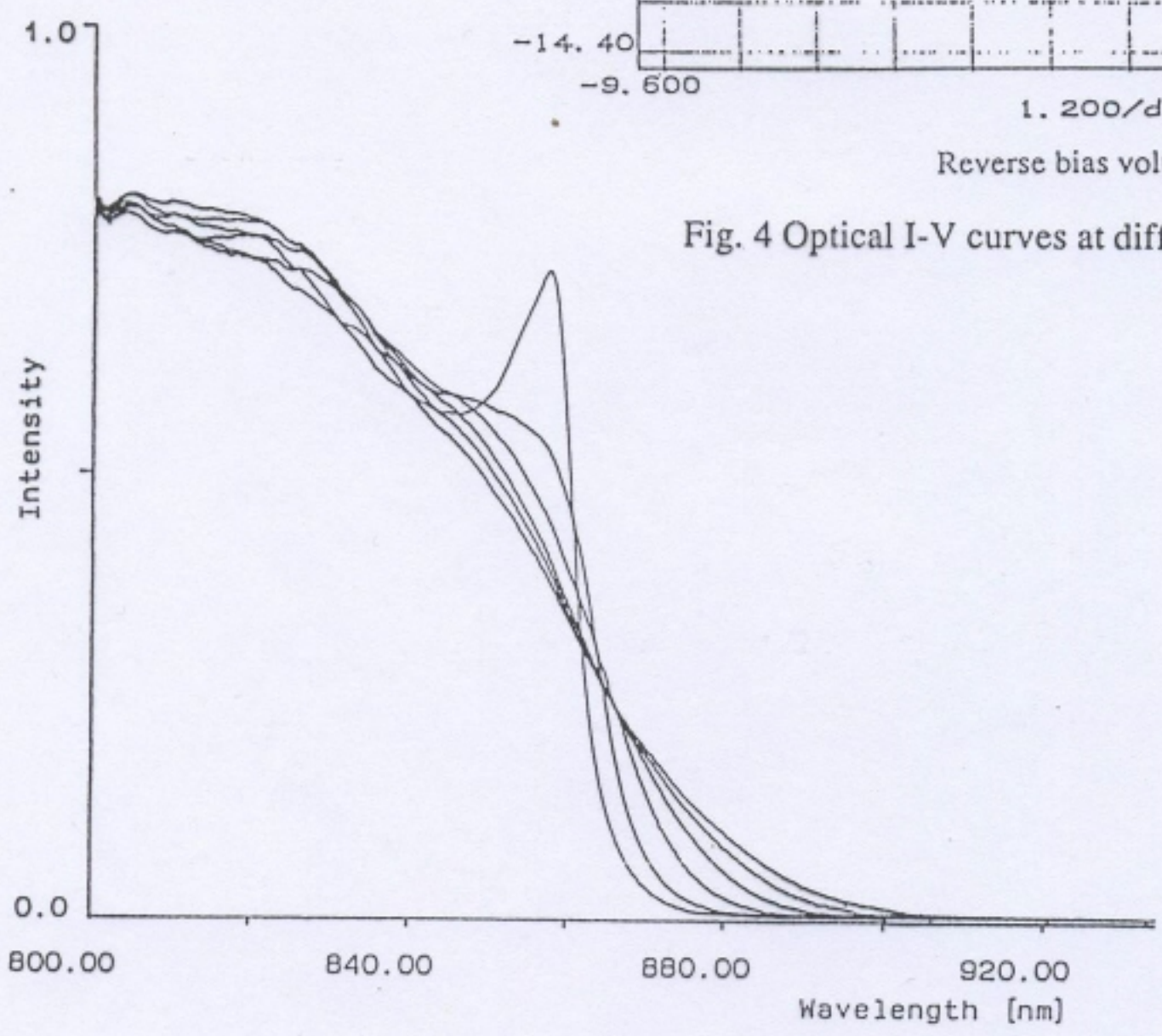


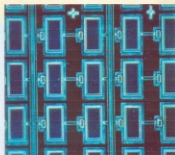
Fig. 5 Photocurrent spectra for varying reverse bias voltages: Curves correspond to 0,2,4,6,8,10V, respectively in descending order from the exciton peak.



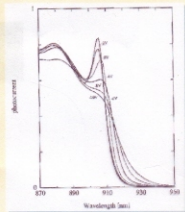
# 연구과제명: 혼성 집적에 의한 VLSI-PIC 회로 설계와 칩의 제작

## ♣ 1차년도 중간 결과

### ♣ PD/S-SEED의 제작

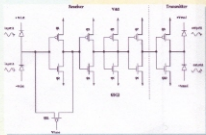


Photograph of 16x8 S-SEED Array

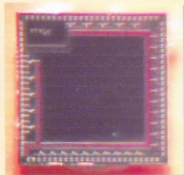


905nm Photocurrent Spectra

### ♣ CMOS-VLSI 회로 설계 및 제작

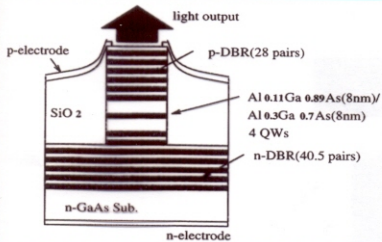


0.8 $\mu$ m CMOS-based Transimpedance Smart-Pixel Optical Receiver

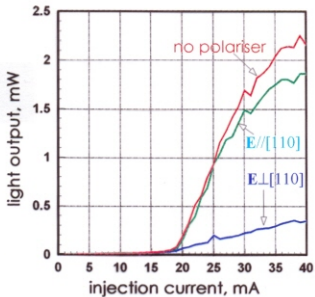


Photograph of the fabricated chip





Schematic of MOCVD-grown VCSEL using conventional DBR

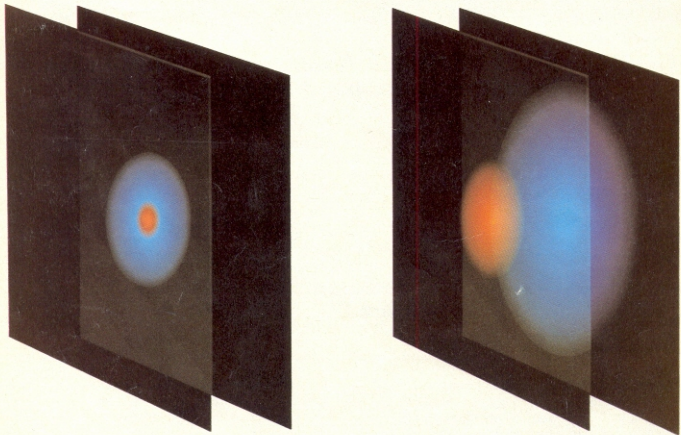


Polarization-resolved LI-curve of a 36 $\mu$ m-diameter VCSEL





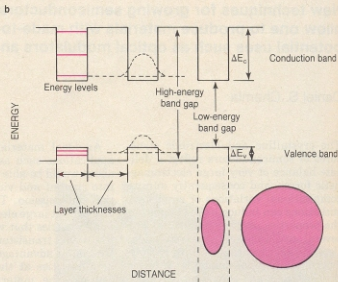
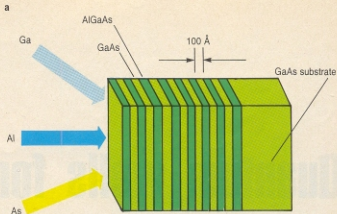




**Quantum confined Stark effect**, in artist's conception. The drawing on the left shows an electron-hole pair, or exciton, trapped in a quantum well in a superlattice material. The left and right planes represent the walls of the well. When an electric field is imposed, right, the electron (blue cloud) and hole (orange cloud) move apart, but the walls of the well are close enough together to prevent the exciton from ionizing.

Figure 1

**Quantum-well structure** and corresponding real-space energy band structure. The schematic diagram in **a** shows compositional profiling in thin layers. The circle in **b** represents the bulk compound, and the ellipse represents an exciton confined in a layer with a low band gap. Figure 2

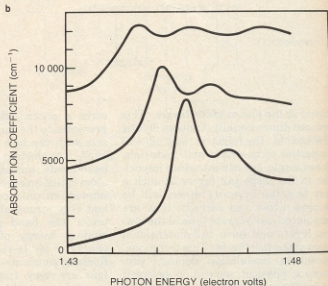
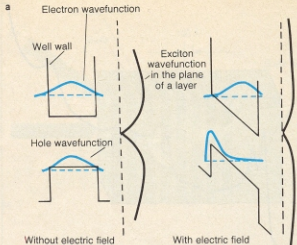


energy gaps and refrac-

and physical compati-  
solutions of various III-  
ake it possible to grow  
s involving several  
e can make heteros-  
high-quality interfaces,  
optical and electronic  
for specific applica-  
structures have not  
ized for more than one  
me, the III-V alloys

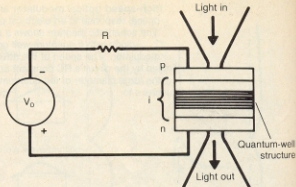


**Excitonic wavefunctions** without and with an applied electric field (a), and the quantum confined Stark shift in an absorption spectrum (b). The wavefunctions illustrate how the walls of a quantum well hold an electron and hole in a bound state, even at applied fields much stronger than the classical ionization field. The absorption spectra are those of a quantum-well structure under three different static electric fields applied normal to the layers. The fields are  $10^4$  V/cm (bottom curve),  $5 \times 10^4$  V/cm (middle curve) and  $7.5 \times 10^4$  V/cm (top curve).  
Figure 4



room temperature. At  
ure the average thermal  
out three times larger  
n binding energy. Note  
that the ionization tem-  
hydrogen atoms is about  
ent measurements with  
optical spectroscopic tech-  
the ionization time of  
quantum-well structures to  
ue to the effects of the  
plasma, the coefficient of  
the index of refraction  
y on the intensity of the  
. These dependencies  
asurements with contin-  
er light as well as with  
er pulses. These nonlin-  
several orders of magni-  
than those observed in  
conductors, yet they are  
f as large as the nonlin-  
nced by the selective gen-  
itons with femtosecond

**Self-electro-optic device** and plots showing its optical bistability. The device in the schematic diagram shows optical bistability when it is connected to a simple resistive load. Figure 6



was only about one micron thick; longer light paths increase the attenuation considerably.

**Self-electro-optic devices.** When a photon is absorbed in a quantum confined Stark effect p-i-n structure, it generates an electron-hole pair that is separated by the field; here the modulator behaves like a photodetector of unit quantum efficiency. The ability of such a p-i-n device to act as both a modulator and a photodetector provides an internal feedback mechanism when the device is connected to an electronic circuit. This is the basis of a new category of devices, known as self-electro-optic devices, that can operate as optical gates with very low switching energy, self-linearized modulators and optical level shifters.<sup>20</sup>

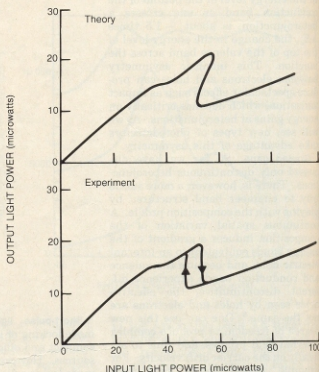
The optical gate represented in figure 6a operates as follows: One applies just enough voltage to the device to shift the absorption edge so that there is little absorption at the exciton peak; then one directs a light beam of varying intensity onto the device. As the beam's intensity increases, it generates a photocurrent that induces a voltage drop across the resistor. The voltage across the device decreases, the edge shifts back and the absorption increases, increasing the photocurrent. This cycle continues until the device switches to a state of low transmission. The switch back to a highly transmitting state does not occur at the same incident intensity because the self-electro-optic device is now absorbing. Therefore the gate response, shown in figure 6b, is an optical hysteresis loop.

The self-electro-optic devices demonstrated to date typically have total switching energies of 20 fJ per square micron. This switching energy is only one-sixth that reported for any other optically bistable device, despite the fact that self-electro-optic devices operate without resonant cavities. The total switching energy comprises two parts: resonant optical energy, which accounts for about 20% of the total, and electrical energy, which accounts for the other 80%. Self-electro-optic devices are compatible with other III-V semiconductor technologies, and should fit into large-scale integrated arrays.

**High-gain avalanche photodetectors** can be built from a solid with a large difference between the rates at which electrons and holes create electron-

hole pairs throughout impact ionization. In gallium arsenide, unfortunately, the two ionization rates are about the same. Furthermore, avalanche multiplication is intrinsically a noisy process because of the randomness of the ionization events, and that causes statistical fluctuations in the gain. New concepts based on quantum-well and graded-gap structures have overcome these obstacles. Figure 7a shows the band structure of a p-i-n diode that contains a quantum-well structure in its intrinsic region. When a hot electron enters a gallium arsenide quantum well, it suddenly gains an energy  $\Delta E_c$ . The ionization threshold for electrons is thus reduced from  $\Delta E_{th}$  to  $\Delta E_{th} - \Delta E_c$ , whereas for the holes it is reduced to  $\Delta E_{th} - \Delta E_v$ . Because the ionization rates depend exponentially

b

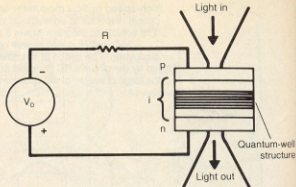


on the thresholds, one can greatly enhance the ratio of electron and hole ionization rates. AlGaAs-GaAs avalanche photodetectors have shown<sup>21</sup> ratios as large as seven. The performances can be improved further by using a sawtooth profile with regions of linear grading followed by abrupt steps, as shown in figure 7b. When one applies a static field to the structure, figure 7c, the impact ionization events occur at each step deterministically, and preferentially for the electrons. The resulting multiplication processes are no longer random, and the gain is almost noise free. The graded-gap structure acts as a solid-state photomultiplier, with the steps in the energy bands corresponding to the dynodes of a traditional photomultiplier tube.<sup>21</sup>

**Fast transistors.** The transit time of



**Self-electro-optic device** and plots showing its optical bistability. The device in the schematic diagram shows optical bistability when it is connected to a simple resistive load. Figure 6



was only about one micron thick; longer light paths increase the attenuation considerably.

**Self-electro-optic devices.** When a photon is absorbed in a quantum confined Stark effect p-i-n structure, it generates an electron-hole pair that is separated by the field; here the modulator behaves like a photodetector of unit quantum efficiency. The ability of such a p-i-n device to act as both a modulator and a photodetector provides an internal feedback mechanism when the device is connected to an electronic circuit. This is the basis of a new category of devices, known as self-electro-optic devices, that can operate as optical gates with very low switching energy, self-linearized modulators and optical level shifters.<sup>20</sup>

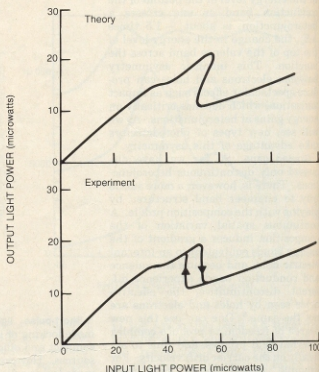
The optical gate represented in figure 6a operates as follows: One applies just enough voltage to the device to shift the absorption edge so that there is little absorption at the exciton peak; then one directs a light beam of varying intensity onto the device. As the beam's intensity increases, it generates a photocurrent that induces a voltage drop across the resistor. The voltage across the device decreases, the edge shifts back and the absorption increases, increasing the photocurrent. This cycle continues until the device switches to a state of low transmission. The switch back to a highly transmitting state does not occur at the same incident intensity because the self-electro-optic device is now absorbing. Therefore the gate response, shown in figure 6b, is an optical hysteresis loop.

The self-electro-optic devices demonstrated to date typically have total switching energies of 20 fJ per square micron. This switching energy is only one-sixth that reported for any other optically bistable device, despite the fact that self-electro-optic devices operate without resonant cavities. The total switching energy comprises two parts: resonant optical energy, which accounts for about 20% of the total, and electrical energy, which accounts for the other 80%. Self-electro-optic devices are compatible with other III-V semiconductor technologies, and should fit into large-scale integrated arrays.

**High-gain avalanche photodetectors** can be built from a solid with a large difference between the rates at which electrons and holes create electron-

hole pairs throughout impact ionization. In gallium arsenide, unfortunately, the two ionization rates are about the same. Furthermore, avalanche multiplication is intrinsically a noisy process because of the randomness of the ionization events, and that causes statistical fluctuations in the gain. New concepts based on quantum-well and graded-gap structures have overcome these obstacles. Figure 7a shows the band structure of a p-i-n diode that contains a quantum-well structure in its intrinsic region. When a hot electron enters a gallium arsenide quantum well, it suddenly gains an energy  $\Delta E_c$ . The ionization threshold for electrons is thus reduced from  $\Delta E_{th}$  to  $\Delta E_{th} - \Delta E_c$ , whereas for the holes it is reduced to  $\Delta E_{th} - \Delta E_v$ . Because the ionization rates depend exponentially

b



on the thresholds, one can greatly enhance the ratio of electron and hole ionization rates. AlGaAs-GaAs avalanche photodetectors have shown<sup>21</sup> ratios as large as seven. The performances can be improved further by using a sawtooth profile with regions of linear grading followed by abrupt steps, as shown in figure 7b. When one applies a static field to the structure, figure 7c, the impact ionization events occur at each step deterministically, and preferentially for the electrons. The resulting multiplication processes are no longer random, and the gain is almost noise free. The graded-gap structure acts as a solid-state photomultiplier, with the steps in the energy bands corresponding to the dynodes of a traditional photomultiplier tube.<sup>21</sup>

**Fast transistors.** The transit time of

# Photonic switching technologies and players

Switching method	Photonic devices	Developers	Current status (devices and systems)	Advantages/disadvantages
<b>Space division</b>				
Guided-wave	Directional couplers	AT&T Co.; LM Ericsson, Stockholm, Sweden; Fujitsu Ltd.; NEC Corp.; and NTT Corp., Tokyo	4-by-4, 8-by-8 prototype devices available; research lab prototype systems	Bandwidth transparent/small-scale integration; difficult synchronization and control
	Digital switches	Ericsson		
	On-off shutters	Optivision Inc., Davis, Calif.	16-by-16 product available	
Free-space	SEED technology	AT&T; University College, London	Products available; system demonstrators	Digital devices/high switching energy; difficult optomechanical packaging technology
	Pnpn technology (DOES, VSTEP, EARS, LAOS)	AT&T; Colorado State University, Fort Collins; NEC; NTT; University of New Mexico, Albuquerque; University of Southern California, Los Angeles	Research prototype devices; research lab experimental systems	
	Smart pixels	AT&T; NEC; NTT; University College, London; University of Southern California	Simple research prototype devices; research lab experimental systems	
<b>Time division</b>				
Time-slot interchange	Directional couplers, fiber delay lines	AT&T, NEC, University of Colorado, Boulder	Prototype devices available; research lab experimental systems	Bandwidth-transparent/small-scale integration; difficult synchronization and control
Multiple-access	Star couplers, tunable lasers, tunable receivers	AT&T; Princeton University, New Jersey		
<b>Wavelength division</b>				
Wavelength interchanger	Star couplers, tunable lasers, tunable receivers	NEC	Prototype devices available; research lab experimental systems	Bandwidth-transparent/small-scale integration; difficult synchronization and control
Multiple-access	Star couplers, tunable lasers, tunable receivers	AT&T; Bellcore, Livingston, N.J.; NEC; NTT; CSELT, Columbia University, New York City		
<b>Multiple division</b>				
Time-space-time	Directional couplers, fiber delay lines	AT&T	Prototype devices available; research lab experimental systems	Bandwidth-transparent/small-scale integration; difficult synchronization and control
Wavelength-space-wavelength	Star couplers, tunable lasers, tunable receivers	NEC		
Packet switching	Star couplers, tunable lasers, tunable receivers	AT&T, Bellcore		
	Smart pixels	AT&T; University College, London; University of Southern California	Research devices; research lab experimental systems	Digital devices/difficult optomechanical packaging technology

SEED = self-electro-optic-effect device  
 DOES = double heterostructure optoelectronic switch.  
 VSTEP = vertical surface transmission electrophotonic.

EARS = excite-absorptive reflection switch.  
 LAOS = light-amplifying optical switch.  
 CSELT = Centro Studi e Laboratori Telecomunicazioni SpA (Telecommunications Research and Study Center), Turin, Italy.





AT&T BELL LABORATORY

At AT&T Bell Labs, Alan Huang (above) continues his effort to build the first full-blown optical digital computer. Bell researchers David Miller (right) and Jill Henry (far right) are pioneering the self-electrooptic effect devices (SEEDs) that will be the basis for optical gates used in the system.



AT&T BELL LABORATORY



(No 75) March 1990

The International Newspaper of Optical and Optoelectronic Applied Science and Engineering

## OPTICAL COMPUTER: Is concept becoming reality?

This issue's Focus

*Microlithography*  
(see pages 12 - 14)

### Digital optical processor demonstrated

AT&T scientists announced on January 29 that they had succeeded in building the world's first digital optical processor. "The digital optical processor is a technological milestone," said William H. Ninke, director of the Information Systems Research Laboratory at AT&T Bell Laboratories. "This wireless processor uses lasers to transmit information internally and employs optical devices to process the information." The optical processor demonstrated at Bell Labs operates at 1 million cycles per second, less than most personal computers. But AT&T scientists are optimistic that an optical computer operating at several hundred million cycles per second—faster than most supercomputers—is possible in the near future.

The switching is handled by S-SEEDs (Symmetric Self-Electro-optic Effect Devices), optical switches with a potential speed of 1 billion operations per second using a switching energy of about 1 picojoule. They are based on GaAs-AlGaAs technology and are fabricated by molecular beam epitaxy. Each device is 5  $\mu\text{m}$  square and contains two mirrors with controllable reflectivity (see interview). There are 32 S-SEEDs on each of four arrays within the processor. Each S-SEED can drive two inputs.

Each array contains two 10-milliwatt modulated laser diodes (850 nm) that can emit many separate beams to provide communications between the arrays.



### Alan Huang research report

Alan Huang is head of the Optical Computing Research Department at AT&T Bell Labs, where the first optical processor was built. He was interviewed by Frederick Su, SPIE Technical Consultant, for OE Reports.

*Other than the speed of light, what is the main difference between photonic processors compared to electronic processors?*

It has nothing to do with the speed of light. It has more to do with the number of connections. Right now, processors are categorized as 16 bit, 32 bit, and that really refers to the width of the data highway. With optics, I believe, we can push the width of this data highway to 1,000 to 10,000 bits wide.

*When you say data highway, the analogy there is like a 16-*

*lane highway?*

**Yes.** In other words, they move 16 bits around at a time.

*With the optical processors you can move 1,000-10,000 bits at the same time?*

**Yes.** If you look at current computers, they are slowed down because they have to time-share the connections. The analogy I have used is much like the island of Manhattan where they

(continued on page 2)

(continued on page 2)



IEEE SPEC. 2/1992

# Switching to photonics

*Voice, video, and data will eventually be switched by hardware that exploits the interplay of photons and electrons*

**T**elecommunications in the future will rely on light as heavily in switching as it does today on light in transmission. The vast information-carrying capacity of optical fiber will be joined to the astounding connectivity of photonics.

Each new wave of switching hardware will have more photonics embedded in it. In 1995, the first specialized applications will be appearing. By 2000 there may not be purely photonic switching but there certainly will be abundant photonics; for example, photonic links will interconnect printed-circuit boards, multichip modules, and equipment frames. By 2010, optoelectronic switching fabrics could be bringing business community and residential customers alike a panoply of broadband services: video, high-definition television, and switched videotelephone conversations and conferences; fast data file transfers and information retrieval; data exchange for diskless workstations; and animated graphics, for example, all in addition to

land, last October. The focus now in many laboratories is on engineering—increasing capacity and performance while reducing size and cost. Still other concepts are in an early experimental stage.

The work is proceeding along two divergent paths. Guided-wave photonics is better understood and more highly developed. It capitalizes on temporal bandwidth: combining a large number of users into a single physical channel, either through time multiplexing or wavelength multiplexing, in structures like optical fibers and star and directional couplers. These structures are bandwidth transparent (support any bit rate).

The alternative, free-space photonics, exploits spatial bandwidth: serving many users in parallel through many separate channels in structures like lenses, mirrors, holograms, and arrays of optical logic gates or optoelectronic integrated circuits. Essentially, guided-wave photonic switching supports many users on a small number of physical

reconfigur

Ericsson  
AT&T Co.  
offer direct  
eight-by-eig  
able to eig

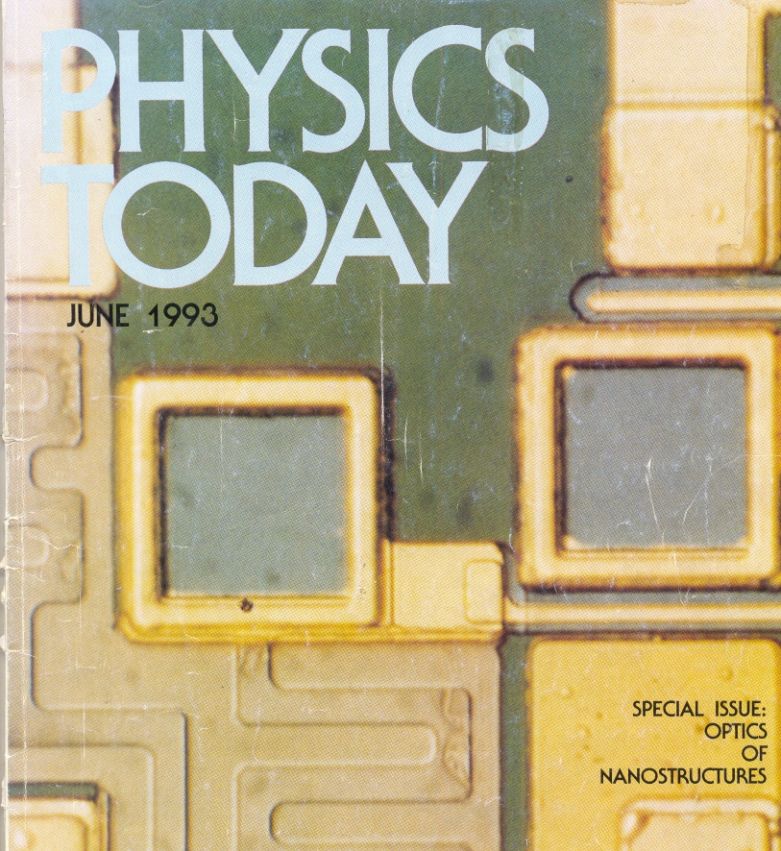
A basic c  
optical inp  
or more ele  
plers are u  
um niobate  
diffused to  
though the  
um arsenic  
phosphide  
voltage on  
optical prop  
the channe  
the cross o  
through to

Up to a p  
plers can be  
factor limit

by the  
it. Bu  
by spe  
polog  
Benes  
loss to  
ar) in  
keep  
come  
A fu  
talk.  
netwo  
two in  
activ

For future photonic switching offices, the aggregate bit rate will be an amazing 1 terabit per second

# PHYSICS TODAY

A microscopic image of a microchip, showing various square and rectangular structures, likely representing nanoscale components or devices. The structures are arranged in a grid-like pattern, with some appearing as raised or recessed areas. The background is a dark, textured surface, possibly the substrate of the chip.

JUNE 1993

SPECIAL ISSUE:  
OPTICS  
OF  
NANOSTRUCTURES